New antimicrobials targeting bacterial RNA polymerase holoenzyme assembly identified with an *in vivo* BRET-based discovery platform

Sara Sartini[1,2], Elisabetta Levati[1], Martina Maccesi[3], Matteo Guerra[1,4], Gilberto Spadoni[5], Stéphane Bach[6], Monica Benincasa[7], Marco Scocchi[7], Simone Ottonello[1], Silvia Rivara[8], Barbara Montanini[1*]

[1]Laboratory of Biochemistry and Molecular Biology, Department of Chemistry, Life Sciences and Environmental Sustainability, University of Parma, 43124 Parma, Italy.
[2]Interdepartmental Research Centre Biopharmanet-Tec, University of Parma, 43124 Parma, Italy;
[3]Department of Chemical and Pharmaceutical Sciences, University of Ferrara, 44121 Ferrara, Italy.
[4]present address: European Molecular Biology Laboratory (EMBL), Cell Biology & Biophysics Unit, 69117 Heidelberg, Germany
[5]Department of Biomolecular Sciences, University of Urbino "Carlo Bo", 61029 Urbino, Italy.
[6]Sorbonne Université, CNRS, UMR 8227, Integrative Biology of Marine Models, Team Physiology and Cell Fate, Station Biologique de Roscoff, CS 90074, 29688 Roscoff Cedex, France
[7]Department of Life Sciences, University of Trieste, 34128 Trieste, Italy.
[8]Department of Food and Drug, University of Parma, 43124 Parma, Italy.

[*] Correspondence: barbara.montanini@unipr.it

ABSTRACT

Bacterial resistance represents a major health threat worldwide and the development of new therapeutics, including innovative antibiotics, is urgently needed.

We describe a discovery platform, centered on *in silico* screening and *in vivo* Bioluminescence Resonance Energy Transfer in yeast cells, for the identification of new antimicrobials that by targeting the protein-protein interaction between the β'-subunit and the initiation factor σ^{70} of bacterial RNA polymerase, inhibit holoenzyme assembly and promoter-specific transcription. Out of 34,000 candidate compounds, we identified seven hits capable of interfering with this interaction. Two derivatives of one of these hits proved to be effective in inhibiting transcription *in vitro* and growth of the Gram-positive pathogens *Staphylococcus aureus* and *Listeria monocytogenes*. Upon supplementation of a permeability-adjuvant, one derivative also effectively inhibited *Escherichia coli* growth.

Based on the chemical structures of these inhibitors, we generated a ligand-based pharmacophore model that will guide the rational discovery of increasingly effective antibacterial agents.

INTRODUCTION

Antibiotic resistance is becoming a major health problem worldwide. According to the World Health Organization, we will soon be facing a so-called 'post-antibiotic era', in which common infections and minor injuries can once again kill (*1*).

Multiple mechanisms, such as masking or modification of the target to make it resilient to antibiotic-mediated inhibition, as well as increased efflux, impaired internalization and/or enzymatic modification of antimicrobial compounds are involved in the development of antibiotic resistance (*2–6*). Two other major determinants of the antibiotic crisis are the abuse/misuse of antimicrobials and the 'unproductivity' of the antibiotic discovery pipeline. In fact, most of the presently available antibiotics have been discovered decades ago and are focused on a relatively small number of biological targets, most notably the ribosome, cell wall biosynthesis and, to a lower extent, DNA replication.

A somewhat underexploited, but fully validated antibiotic target is bacterial RNA polymerase (RNAP), which in response to the need for new antibiotics is re-gaining momentum as an attractive antimicrobial target, also thanks to the increasing availability of novel inhibitory compounds and high-resolution RNAP as well as RNAP-inhibitor structures. The potential of RNAP as a valuable antibiotic target stems from its essential biological function and high degree of conservation across bacterial species, yet with a sufficient divergence from its eukaryotic counterpart that makes cross-inhibition and toxicity fairly rare events. Indeed, two RNAP inhibitors, rifampin and lipiarmycin, targeting distinct RNAP active site regions (*7–9*), have been approved for clinical use. Despite their undisputable efficacy, mutations can lead to acquired drug resistance and failure of antibiotic treatment to cure infections. Resistance-conferring mutations can also affect the treatments with newly discovered RNAP inhibitors, including multiple compounds, in addition to lipiarmycin, that target the RNAP switch region, and the recently discovered natural nucleoside analog pseudouridimycin (PUM) (*10–14*).

In bacterial cells RNAP is present as both a catalytically active, but promoter-blind, core enzyme (RNAPc) formed by five subunits (α_2, β, β', and ω) and a holoenzyme form (RNAPh), which upon sigma factor incorporation (e.g., the primary house-keeping *Escherichia coli* factor σ^{70}) gains the ability to recognize promoter sequences and to transcribe RNA in a promoter-specific manner. Because of its absolute requirement for productive and specific transcription, the RNAPc-σ^{70} interaction represents another attractive target for RNA synthesis inhibition. This relies on a specific protein-protein interaction (PPI), centered on the clamp helix (CH) region of the RNAPc β'-subunit and the $\sigma_{2.2}$ region of the σ factor. Key amino acid residues likely involved in such interaction have been revealed by site-directed mutagenesis experiments (*15–18*) and by the multiple 3D structures of bacterial RNAP holoenzymes (1L9U, 1Iw7, 4YG2 and references within) (*19–21*). These include both polar amino acids (*E. coli* amino acid residues Arg275, Arg278 and Arg281 in the β'-subunit and Asp403 and Glu407 in σ^{70}) as well as hydrophobic amino acid residues (Leu282 and Met298 in the β'-subunit and Ile410 and Leu402 in σ^{70}). Compensatory amino acid substitutions in both RNAP subunit regions are thus presumably required for the acquisition of resistance while preserving bacterial cell viability.

Following the proof-of-principle demonstration that designed peptides mimicking the $\sigma_{2.2}$ region can prevent RNAPh formation and inhibit *in vitro* transcription (*22*), the construction of a structure-based pharmacophore model led to the identification of two compounds (GKL003 and C5, **1** and **2** in Table 1) that by binding to the β'-subunit interfere with *in vitro* transcription initiation at nM concentrations (*17, 23*). However, when tested for their ability to inhibit bacterial growth, both compounds were found to exhibit antimicrobial activity at

500–100,000 fold higher concentrations, an observation that may be explained by their poor solubility and/or permeability properties. Therefore, while confirming the β'-σ^{70} interaction as a viable target for the development of novel antimicrobials, these results, which have been primarily derived from *in vitro*-based screenings, leave room for a number of improvements. Considering the sub-optimal properties of known β'-σ interaction inhibitors, and in particular their very poor (or lack of) antibacterial activity (*17, 23*), we decided to explore an expanded chemical space, searching for inhibitors belonging to new chemical classes with more promising antibacterial properties.

With this goal in mind, we developed and optimized a Bioluminescence Resonance Energy Transfer assay in yeast (yBRET) as an *in vivo* tool for the screening of large candidate compound libraries (*24–26*). yBRET is based on resonance energy transfer between a "donor" luciferase and an "acceptor" fluorescent protein fused to the proteins of interest, both expressed inside yeast cells. If the two proteins interact, energy transfer between the two partners takes place, leading to acceptor fluorophore excitation and the emission of a quantifiable fluorescence (BRET) signal, which will decrease in the presence of an interaction inhibiting compound. yBRET has two favorable features, which are particularly advantageous for the screening of candidate antimicrobial compound libraries: i) the capacity to select for potentially cell-permeant compounds due to its intracellular mode of operation; ii) the ability to immediately detect compounds that are toxic to eukaryotic cells based on the loss of luciferase luminescence.

In this study, yBRET screening of about 5,000 candidate compounds, *in silico* selected from a larger (≈34,000) compounds library, allowed the identification of seven new hits interfering with the RNAP β'-σ^{70} interaction. Four of these hit compounds were independently validated in ELISA and proved to preferentially bind β'-subunit. Two derivatives of one of these hits displayed an *in vitro* RNAP inhibitory activity slightly lower than that of the best available compound (**1**), but inhibited *E. coli* and *Staphylococcus aureus* growth at a more than one order of magnitude lower concentration (50–100 μM vs 2 mM) (*17*). Based on the diverse molecular structures of these newly discovered β'-σ^{70} interaction inhibitors, we designed a pharmacophore ligand-based model and delineated its mode of binding to the CH region of the RNAP β'-subunit.

RESULTS AND DISCUSSION

Reconstitution of the β'-σ^{70} interaction in a yBRET format

Available 3D structures of the *E. coli* RNAPh (*19*) and knowledge of the amino acid residues involved in the β'-σ^{70} interaction (*17*) guided the design of the two protein partner constructs for the BRET assay. Given the lack of prior studies using the isolated σ$^{70}_{2.2}$ domain for RNAPh reconstitution, we initially focused on full-length σ^{70} and on two different portions of the β' clamp domain overlapping the β' CH region comprised between amino acid residues 1–334 and 220–334, respectively.

In our yBRET set-up the engineered deep-sea shrimp luciferase NanoLuc® (NLuc) is utilized as donor protein and the Yellow Fluorescent Protein (YFP) as acceptor: the protein targeted by the inhibitor (β') is fused to the acceptor (YFP) and is constitutively expressed, while expression of the donor-fusion protein (σ^{70}-NLuc) is under the control of the yeast *GAL1* promoter and induced after the addition of the candidate inhibitor compound, to allow for binding of the inhibitor to its target before interaction reconstitution and complex formation (Figure 1A).

BRET signals were measured in the hyper-permeable *Δerg6* yeast strain in order to maximize luciferase substrate and candidate compound internalization. The YFP-β' fusion proteins always gave weaker signals compared to the oppositely oriented β'-YFP fusions, whereas the orientation of the NLuc donor relative to σ^{70} affected yBRET signal strength to a much lower extent. The shorter (aa. 220–334) β' CH region fragment yielded lower BRET signals compared to the longer (aa. 1–334) fragment. This is likely due to the lack of the β' portion comprised between aa. 41–47, which being also involved in the interaction with the aa. 446–453 region of σ^{70} (*E. coli* 4YG2), might strengthen the overall interaction but might also be required for a correct folding and positioning of the CH region. Thus, the NLuc-σ^{70} / β'(1–334)-YFP pair, which produced the highest BRET signal, was chosen as the best combination for subsequent experiments (Figure 1A).

To be reliably employed for compound screening, the BRET platform must be optimized for signal sensitivity and the specificity of the interaction has to be verified. In the yeast co-transformant expressing NLuc-σ^{70} and β'(1–334)-YFP, the BRET signal increased with increasing galactose concentrations up to saturation (not shown) and the minimum galactose concentration (0.5%) yielding the most stable BRET signal (114.1 ± 6.9 mBRET) was thus chosen for subsequent experiments. To verify the specificity of the BRET-reconstituted β'-σ^{70} interaction, we mutated specific amino acid residues previously shown to be critical for this interaction (*15*–*19*). As shown in Figure 1B, the σ^{70} Q406K-E407A double-mutant caused an almost complete loss of the BRET signal, and a 60% reduction of the BRET signal was observed with the β' R275A-R278A double-mutant.

Next, we ran a donor saturation assay to determine whether the observed BRET signal results from random (non-specific) contacts or from a specific PPI. To this end, we swapped the promoters previously utilized for NLuc-σ^{70} and β'(1–334)-YFP expression, in order to achieve inducible, galactose concentration-dependent expression of graded amounts of the β'-YFP acceptor partner in the presence of a fixed (constitutively expressed) amount of the NLuc donor-σ^{70} partner. Under these conditions, the BRET signals measured in the presence of increasing inducer concentrations fitted a hyperbolic curve, as expected for a specific PPI (*27*), with both the wild type and the R275A-R278A mutated versions of the 1–334 β'-subunit fragment (Figure 1C). Altogether, these results demonstrate the specificity of the β'-σ^{70} interaction reconstituted inside BRET-engineered yeast cells.

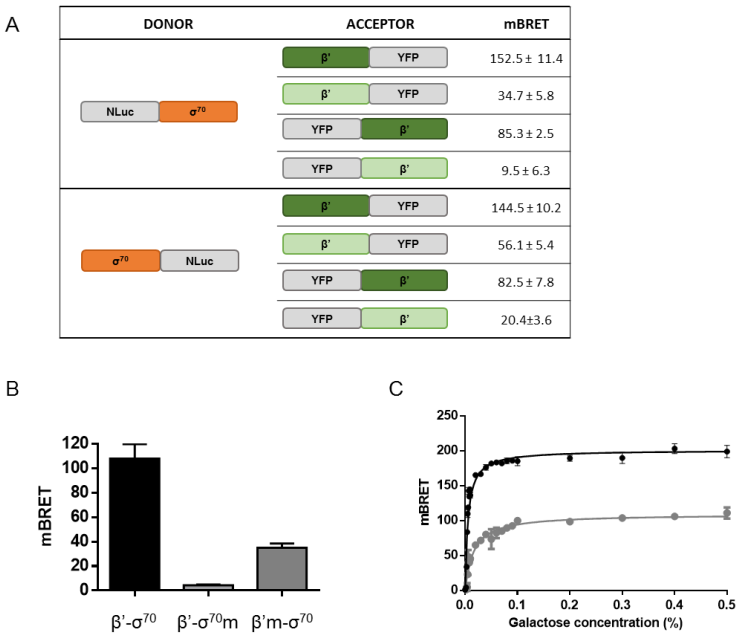

Figure 1. yBRET reconstitution of the β'-σ^{70} interaction and evaluation of BRET signal specificity. (A) Outline of the different fusion constructs and of the corresponding BRET signals. β' (dark green: aa. 1–334; light green: aa. 220–334) and σ^{70} (orange) were joined to the N- and the C-terminus of NLuc and YFP (light gray); (B) BRET signal decrease associated to mutant versions of σ^{70} (Q406K-E407A; σ^{70}m) and β' (R275A-R278A; β'm) compared to the wild-type form of both interactors (β'-σ^{70}). Donor fusion proteins were induced in the presence of 2% (A) or 0.5% (B) galactose. (C) Donor saturation assay of the β'-σ^{70} interaction. In the latter assay, the promoters were swapped to obtain the inducible expression of the YFP fusion proteins (using the indicated galactose concentrations) and the constitutive expression of NLuc-σ^{70}. Black: wild-type β'(1–334)-YFP; grey: β'm(1–334)-YFP. Data are the mean of three replicates; error bars represent SD.

Functional evaluation of the yBRET screening platform

To validate the yBRET screening platform, we initially used GKL003 and C5 (**1** and **2** in Table 1) as reference compounds previously shown to interfere with the β'-σ^{70} interaction (*17, 23*). The results, however, were largely unsatisfactory, since compound **1** was poorly soluble and displayed a milky consistence when dissolved in yeast synthetic medium at concentrations higher than 10 μM, while compound **2** absorbed at 480 nm and emitted at 530 nm, with a significant overlap to the NLuc and YFP spectra that made BRET measurements unreliable. To evaluate the ability of yBRET to specifically identify compounds that inhibit the β'-σ^{70} interaction, and given the presence of an indole ring in GKL003 and its *in vitro* active derivatives, we screened an in-house mini library of 27 indole derivatives (10 mono-indoles and 17 bis-indoles, compounds **3**–**29** in Supplementary Table 1) (*28–31*) which were assayed under optimized yBRET conditions and compared with the corresponding results obtained with the use of ELISA. As shown in Supplementary Figure 1A, six of the tested compounds caused BRET signal reduction (up to 50%) without any sign of toxicity.

The yBRET-positive compounds **5** and **15**–**18**, along with two inactive compounds from the same mini-library (the mono-indole **3** and the bis-indole **21**) and the reference compounds **1** and **2** were thus tested for their ability to interfere with the β'-σ^{70} interaction in a cell-free assay based on ELISA. yBRET-positive molecules inhibited the β'-σ^{70} interaction also in ELISA, whereas **3** and **21** were almost completely inactive, thus indicating the reliability of our yBRET-based discovery platform (Supplementary Figure 1B). Compounds **5** and **15** were further evaluated and compared with reference compound **1** in a dose-response ELISA. As shown

in Supplementary Figure 1C, they were found to be approximately three-times less potent, with IC_{50} values of 43.8 μM (**5**) and 54.5 μM (**15**), compared to an IC_{50} of 17.6 μM for compound **1**.

Virtual screening campaign for the pre-selection of candidate β'-σ^{70} interaction inhibitors

The 'Open Collection Scaffolds' library from Compounds Australia (Griffith University) (*32*), comprising a total of 33,999 commercially available compounds, was used as a repository for the *in silico* selection of approximately 5,000 candidate β'-σ^{70} interaction inhibitors to be subjected to the yBRET screening. Since low MW compounds are less likely PPI inhibitors (*33*), the library was first filtered by retaining compounds with MW≥ 250. Next, we performed multiple virtual screening runs on the filtered library by applying ligand-based and structure-based selection methods according to the workflow reported in Supplementary Figure 2A. Given the limited information on the key structural elements that are critical for β'-σ^{70} interaction disruption, and the medium resolution of the available crystal structures, different selection methods were applied to maximize the possibility of retrieving biologically active compounds. A structure-based selection was first performed by evaluating the fitting of individual compounds to a pharmacophore model built on the 2.2 region of σ^{70}. This pharmacophore model contains seven sites corresponding to the most important amino acid residues of the β'-σ^{70} contact region, as revealed by 3D structure and mutagenesis data (*15*–*19*) (Supplementary Figure 2B and 2C). A major difference between the present model and the pharmacophore reported by Ma et al. (*17*) is that the last one was based on a homology model of *Bacillus subtilis* RNAP while our pharmacophore was built on the crystal structure of *E. coli* RNAPh (PDB: 4YG2). Compared to the 4-site model by Ma, our model has additional sites placed on σ^{70} residues Gln406, Leu402 and Asp403. Ligand-based selection was then carried out taking into account four different criteria: i) Shape-screening performed using reference compound **1** in a minimum-energy extended conformation as query (Supplementary Figure 2D). ii) Mutagenesis data indicated the importance of $\sigma_{2.2}$ acidic residue Glu407 (*18*) for the interaction with β'. Further to this point, reference inhibitor **2,** which binds to the β'-subunit, contains a carboxylic group. Therefore, a sub-structure search was conducted to retrieve the 367 compounds bearing a carboxylate group. iii) Given the presence of an indole ring in several β'-σ^{70} interaction inhibitors (*34*), comprising reference compound **1**, the 876 indole derivatives present in the library were also selected. iv) 2D similarity screening based on linear fingerprints using inhibitor **1** as reference structure. Combined use of the above selection criteria led to a final subset of 4960 unique candidate compounds to be subjected to yBRET screening as potential β'-σ^{70} interaction inhibitors.

yBRET screening of the *in-silico* selected compound library

The 4960 compounds selected and retrieved from the 'Open Collection Scaffolds' library were initially screened by yBRET at a fixed concentration of 20 μM, the highest possible concentration allowed by the limited amounts at which the compounds were supplied. Compounds that reduced the BRET signal by at least 15% were retained and re-assayed at the same concentration as well as at a 10 μM concentration. This led to the identification of seven hits belonging to different chemical classes (Table 1).

Table 1: Structure and β'-σ^{70} binding inhibition capacity of reference and hit compounds

Compound	Structure	yBRET % inhibition of binding (20 μM)	ELISA % inhibition of binding (250 μM)	ELISA IC_{50} (μM)
1[a] **(GKL003)**	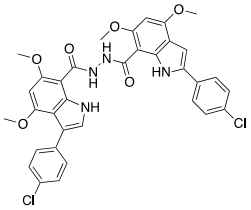	n.a.	84±14	17.6±1.3
2[a] **(C5)**	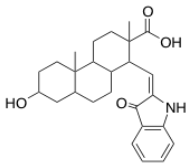	n.a.	46±1[b]	n.a.
30	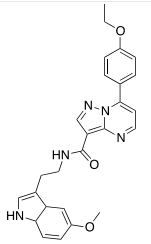	18±2	0[c]	n.a.
31	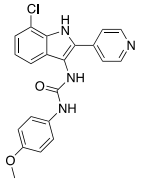	28±1	87±4	16.1±1.1
32	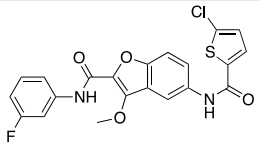	23±2	0[c]	n.a.
33	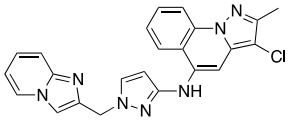	21±6	99±4	11.4±1.1
34	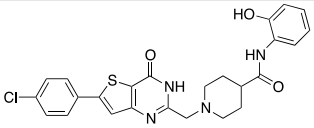	28±3	93±1	11±1.1
35	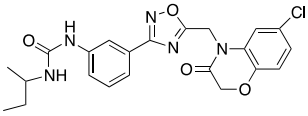	22±1	0[c]	n.a.
36	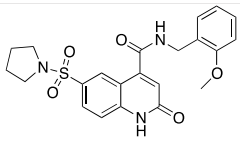	16±5	82±6	91.3±1.2

[a]Compounds **1** (GKL003; (*17*)) and **2** (C5; (*23*)) were used as references.

[b]Compound **2** was assayed at a 500 μM concentration.

[c]Compounds **30**, **32** and **35** were assayed at a 40 μM concentration.

n.a.: not assayed.

To avoid potential batch-to-batch inconsistencies, independent production batches of the seven hits were acquired and subjected to yBRET assay confirmation and ELISA validation (Table 1). Four of the seven yBRET-positive compounds (**31, 33, 34** and **36**) were confirmed as inhibitors of the β'-σ^{70} interaction in ELISA (Table 1), while compounds **30**, **32** and **35** turned out to be insoluble in PBS at concentrations higher than 40 μM and did not display any inhibitory activity when tested at a 40 μM (or lower) concentrations, and were thus not further pursued. The binding inhibition capacity of the four soluble hits was further assessed in a dose-response ELISA, which in the case of compounds **31, 33** and **34** revealed IC_{50} values, ranging from 11.0 μM (**34**) to 16.7 μM (**31**), very similar to the IC_{50} of the reference compound **1** (17.6 μM), but with higher efficacies (98–100% *vs.* 80%) (Table 1 and Supplementary Figure 3). Under the same experimental conditions, compound **36** proved to be the least potent (IC_{50} = 91.3 μM).

Compound **31**, bearing an indol-3-yl-urea scaffold, was further investigated through the acquisition and ELISA testing of 12 commercially available structural analogs (listed in Supplementary Table 2) to evaluate their relative potencies and obtain preliminary information on structure-activity relationships. All indol-3-yl-urea derivatives proved to be active as inhibitors of the β'-σ^{70} interaction (Supplementary Table 2), and nine of them reduced the PPI-associated ELISA signal by more than 80% (Supplementary Table 2). Analysis of the data obtained at a fixed compound concentration suggests that a phenyl substituent on the amide group is preferred to a benzyl substituent at the same position, and that lipophilic substituents linked to the phenyl ring are well tolerated. Likewise, the presence of a 3- or a 4-pyridyl ring at position 2 of the indole ring leads to similar potencies. A dose-response ELISA analysis of three of the best indol-3-yl-urea derivatives (**41**, **43** and **47**) showed very similar potencies (IC_{50} ≈10 μM) for compounds **41** and **43**, which differ only for pyridyl ring substitution, and an IC_{50} of 20.8 μM for compound **47** (Supplementary Table 2 and Supplementary Figure 3).

We then verified the target specificity of the yBRET hits **31**, **33, 34** and **36** and of the indole containing molecules **5**, **15**, and **41**, by replacing β' with σ^{70} as primary interactor in ELISA; compound **1**, previously shown to specifically target the RNAP β'-subunit (*17*), was used as an internal reference for this analysis. As shown in Figure 2, a significant (2–4-fold) reduction of binding inhibition compared to the oppositely arranged ELISA format (i.e., using β' as primary interactor) was observed for all compounds, except for the bis-indole **15**. In accordance with our experimental design, this indicates that the newly discovered inhibitors interfere with the β'-σ^{70} interaction by binding to the RNAP β' subunit.

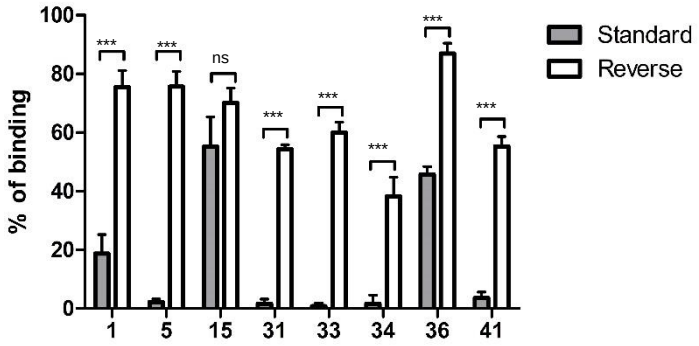

Figure 2. Target specificity of the interaction inhibitors. Comparative forward (β' first, grey bars) and reverse (σ^{70} first, white bars) ELISA analysis of β'-σ^{70} binding inhibition by a subset of preselected compounds. All compounds were tested at a fixed 100 μM concentration. Data, reported as percent binding relative to the DMSO vehicle, are the mean of three replicates; error bars represent SD; ***: two-tailed t-test p-value < 0.001; ns: not significative (p-value > 0.05).

RNAP inhibitory and antibacterial activity

Next, we investigated the ability of the indol-3-yl-urea derivatives (**41**, **43** and **47**), together with the mono-indole **5** and the bis-indole **15** from the in-house mini library, to inhibit promoter-specific RNA transcription. Compound **1**, plus rifampin, served as reference compounds for single-round *in vitro* transcription assays, performed with *E. coli* RNAP under non-competitive inhibition conditions. In the single-round transcription assays the transcription signal is directly proportional to the number of RNAPc-σ^{70} active complexes formed, so the signal decrease measured in the presence of the test compounds is strictly correlated with the inhibition of σ^{70} binding. As shown in Figure 3A, all compounds, except **15**, almost completely inhibited transcription at 50 μM. Dose-response curves were determined for the compounds **43** and **47**, which yielded IC_{50} values (28.6 ± 1.0 μM; and 32.8 ± 1.1 μM, respectively) approximately three times higher than that of reference compound **1** (11.5 μM) (Figure 3B).

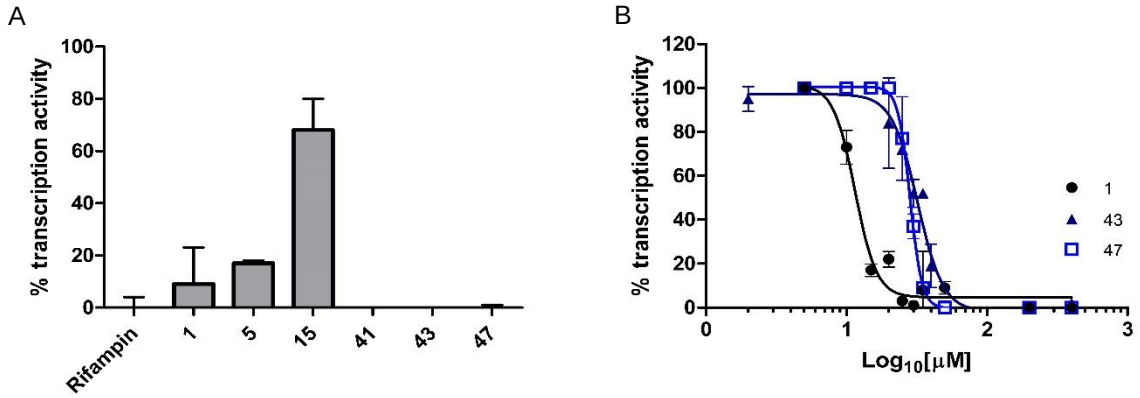

Figure 3. Transcription inhibition. (A) *In vitro* transcription activity measured in the presence of a subset of prevalidated compounds, including reference compound **1**, and Rifampin as a positive control, assayed at a 50 μM concentration. (B) Dose-response curves for a selected subset of compounds. Inhibition curves for hit compounds **43** (Δ) and **47** (□) are shown in blue and light blue, respectively; reference compound **1** (O) is in black. *In vitro* transcription activity is reported as percent relative to the DMSO vehicle. Data are the mean of three replicates; error bars represent SD. See Supplementary Figure 4A and 4B for representative gel images.

In the *in vitro* transcription assay, in the case of reference compound **1** we measured an apparent IC_{50} three orders of magnitude higher than that reported by Ma et al (*17*). This was likely due to the use in our assay of a 20-fold lower RNAPc enzyme: σ^{70} ratio, an experimental parameter previously shown to critically influence the sensitivity and outcome of *in vitro* transcription inhibition assays (*17*). Despite this methodological inter-study difference, overall internally consistent results were obtained for the *in vitro* inhibition capacity (both ELISA and transcription) of reference compound **1** and the newly identified inhibitors.

The same subset of *in vitro* transcription-validated inhibitors, plus the four yBRET hits (**31**, **33**, **34**, **36**) and reference compound **2**, were then assayed for antibacterial activity. This was initially tested on the Gram-positive *B. subtilis* WB800N strain and on the Gram-negative non-pathogenic *E. coli* DH10 T1R strain by monitoring microbial growth in the presence of a fixed concentration of each compound (200 μM; 8 h treatment). As shown in Supplementary Table 3, three compounds (**2**, **43** and **47**) displayed a nearly complete growth inhibitory effect (88–99%) on *B. subtilis*, whereas a much lower growth inhibition (ranging from 28% to 36% for compounds **47**, **43** and **41**) was observed in the case of *E. coli*. This bacterial group-specific difference in efficacy was largely offset by the addition of the outer membrane permeabilizer polymyxin B nonapeptide (PMBN; a non-bactericidal derivative of polymyxin B), suggesting that reduced effectiveness against *E. coli* is likely due to defective compound internalization. In fact, in the presence of 2 μg/ml PMBN, the inhibitory activity on *E. coli* of compounds **41** and **43** raised to 81% and 100%, respectively (Supplementary Table 3). As shown in Supplementary Figure 5, PMBN, at this concentration, did not affect bacterial growth.

Overall, compounds **41**, **43** and **47** proved to be the most active. Compounds **43** and **47** displayed preferential inhibitory activity against *E. coli* and *B. subtilis*, respectively, whereas **41** inhibited growth of both bacteria with a milder efficacy. Importantly, the three compounds retained a significant (33%–60%) inhibitory activity upon prolonged (22 h) culture (not shown) and displayed no (**41**, **43**) or a negligible (5%; **47**) growth inhibition on the unicellular eukaryote *Saccharomyces cerevisiae*, when tested at the same concentration (Supplementary Table 3).

The antibacterial activity of the most potent inhibitors (**43** and **47**) was further assayed at different compound concentrations, monitoring growth inhibition on the same *E. coli* and *B. subtilis* strains every 30 min for 8 h (Figure 4). In this assay, compound **43** proved again to be the most potent against *E. coli*, with a complete growth inhibition down to a 100 μM concentration and a well detectable inhibitory effect even at the lowest (50 μM) concentration (Figure 4A). A significant but somewhat reduced effect, i.e., with a marked drop of inhibitory activity at 50 μM, was observed also on *B. subtilis* (Figure 4D). Compound **47**, instead, displayed a relatively weak inhibitory activity against *E. coli* (Figure 4B) but a high efficacy against *B. subtilis*, with a complete growth inhibition down to a 50 μM concentration and a smaller but still significant effect at 25 μM (Figure 4E). The results of a comparison of the inhibitory capacity of the indol-3-yl-urea derivatives **43** and **47** with reference compounds **1** and **2**, using rifampin as a positive control, are also shown in Figure 4 (panels C-F). All compounds were employed at a fixed concentration (100 μM), and in accordance with previous data (*17, 23*), neither of the reference compounds exerted any appreciable inhibitory effect on *E. coli* and only a weak growth inhibition was observed with compound **2** in the case of *B. subtilis*. As expected, rifampin completely blocked both bacteria and displayed a time-dependent growth inhibition identical to that of compounds **43** and **47** in the case of *B. subtilis*, and to that of compound **43** in the case of *E. coli*. These results are in agreement with those reported for the reference compounds, previously identified solely on the basis of *in vitro* screenings, which failed to inhibit bacterial growth (**1**) or did so (**2**) with low efficacy.

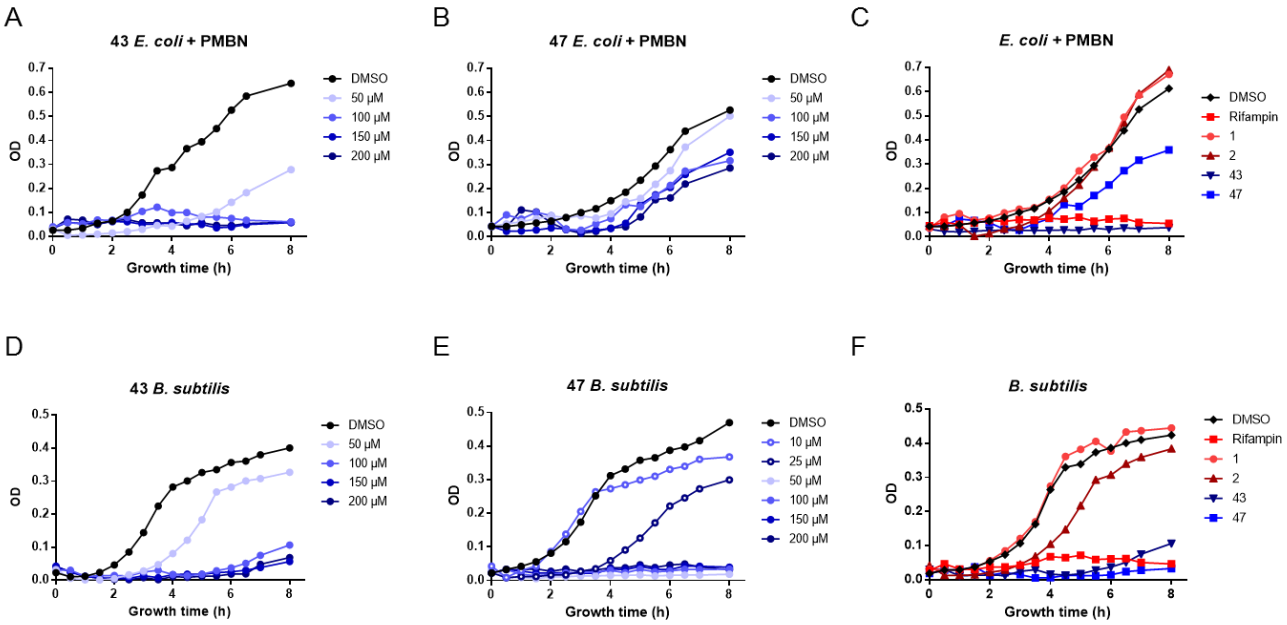

Figure 4. Antibacterial activity. Growth inhibition assays conducted in the presence of different concentrations of compounds **43** (A, D) and **47** (B, E) against *E. coli* DH10 T1R (A, B, C) and *B. subtilis* WB800N (D, E, F), as indicated. Multiple compounds, including Rifampin and reference compounds **1** and **2**, were assayed at a fixed concentration (100 µM) in panels C and F. All assays performed on *E. coli* were supplemented with 2 µg/ml PMBN as indicated; data for the DMSO vehicle only are also reported.

To further investigate the antibacterial activity of the two best compounds (**43** and **47**), additional antibacterial assays were performed. We first determined the Minimum Inhibitory Concentration (MIC) for both compounds against *E. coli* DH10 T1R and *B. subtilis* WB800N, and also against the Gram-positive pathogens *S. aureus* ATCC 25923 and *Listeria monocytogenes* DSM 20600 (Supplementary Table 4). The four bacterial strains were all found to be susceptible to compounds **43** and **47**, with MIC values ranging from 25 to 100 µM (9.5–43 µg/ml). To gain insight on (and distinguish between) a bactericidal *vs.* a bacteriostatic activity of the compounds, we performed a killing assay using as readout the number of residual viable cells after 8 h of treatment. As shown in Figure 5 (A), both compounds effectively killed *E. coli* at a 50 µM and 100 µM concentration after treatment. Both compounds were also bactericidal against *B. subtilis* and the pathogen *L. monocytogenes* (Figure 5B, C) at 100 µM, and particularly compound **47** reduced the number of viable cells also at 50 µM concentration (Figure 5B, C). On the other hand, both compounds only displayed a bacteriostatic effect on *S. aureus* (Figure 5D).

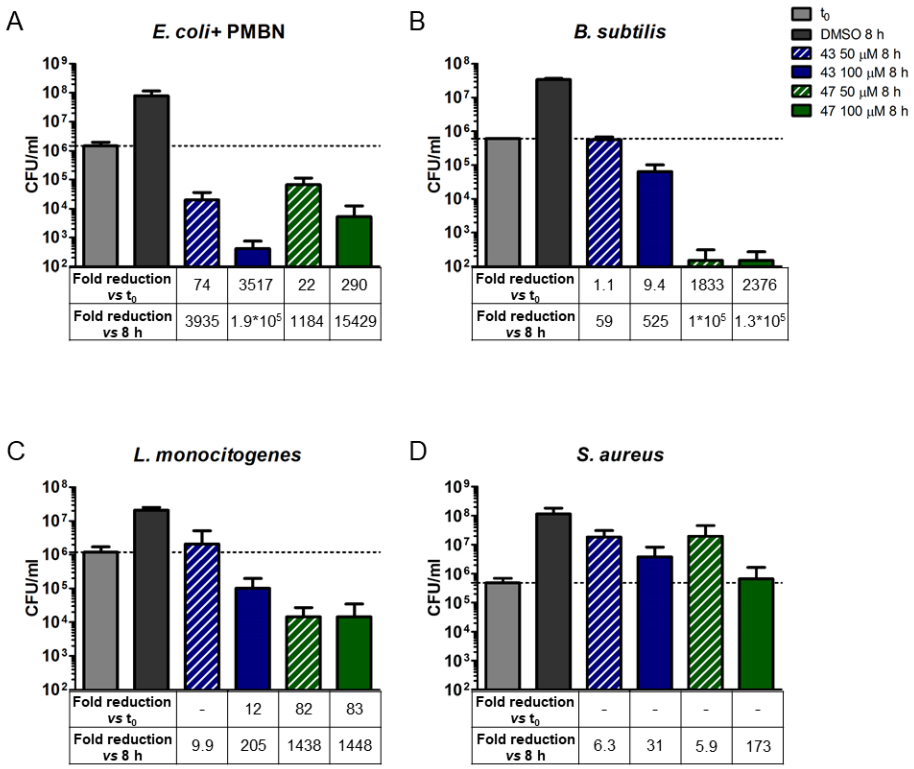

Figure 5. Effect of compounds on bacterial viability**.** Bacterial cell viability, expressed as CFU/ml, was measured at t_0 and after 8 h culture of *E. coli* DH10 T1R (A), *B. subtilis* WB800N (B), *L. monocytogenes* DSM 20600 (C), and *S. aureus* ATCC 25923 (D) in the presence of fixed concentrations (50 μM and 100 μM) of compounds **43** and **47**, or DMSO vehicle. Assays performed on *E. coli* were supplemented with 2 μg/ml of PMBN. Gridlines mark the CFU/ml at t_0. Bactericidal effect, that is evidenced by a decrease in the number of viable cells after treatment compared to initial inoculum, is reported under the histograms as Fold reduction *vs* t_0. Growth inhibition values, relative to the DMSO vehicle (Fold reduction *vs* 8 h), are also reported under the histograms. Data are the mean ±SD of at least three replicates.

As shown by the need for the membrane permeabilizer PMBN in order to achieve an antibacterial effect against *E. coli* and as pointed out by many other studies, in which hyper-permeable *E. coli* mutants were used for testing antibacterial activity (*12, 35*), inhibitor internalization likely represents the main bottleneck in the discovery of new effective antibiotics. Indeed, despite the presence in $\sigma_{2.2}$ of an acidic residue (Glu407) critically involved in the β'-σ^{70} interaction (*18*), and the inclusion of 367 carboxylate group-containing compounds in our candidate compound library, no inhibitor bearing a negatively charged group at physiological pH, and thus presumably unable to cross the hydrophobic core of the membrane, was retrieved by the yBRET screening.

To obtain initial information on cytotoxicity against mammalian cells, we tested the hemolytic activity of compounds **43** and **47** on human erythrocytes. In keeping with the lack of cytotoxicity previously observed in the lower eukaryote *S. cerevisiae*, no or only negligible (less than 2%) hemolysis was detected at the highest tested concentration (200 μM), indicating that both compounds are indeed non-toxic at antibacterial effective concentrations (Supplementary Table 5).

Ligand-based pharmacophore model and β' binding hypothesis

A pharmacophore model was built based on a subset of the active compounds identified through yBRET (**5**, **15**, **33**, **36** and **41**), plus reference compound **1,** representative of the structural diversity of β'-σ^{70} interaction

inhibitors. These compounds share the presence of aromatic portions variably combined with polar groups not ionizable at physiological pH. Active compound **34** was excluded because of the presence of a basic group, not found in any of the other compounds, which could affect binding mode. The pharmacophore model thus obtained is characterized by five pharmacophore sites: two ring sites that accommodate aromatic portions of the compounds, a hydrophobic site, a hydrogen bond acceptor, and a hydrogen bond donor site (outlined in Figure 6 A, B and in Supplementary Figure 6A). All six β'-σ^{70} inhibitors fulfill the requirements of the pharmacophore model, with functional groups chemically consistent with the nature of the pharmacophore sites and proper spatial arrangements. Interestingly, compared to the structure-based pharmacophore built on σ^{70} residues and used for compound selection (Supplementary Figure 2C), this ligand-based model lacks negatively charged sites. This might be explained by the use of yBRET as a primary screening, which requires compound internalization into yeast cells, a process that may be hindered by the presence of negatively charged groups. Likewise, ionized groups might also hamper access to the bacterial cytoplasmic compartment and may thus explain the limited antibacterial activity of compound **2**.

Since no structural information is available on the interaction of β' with a β'-σ^{70} PPI inhibitor, the ligand-based pharmacophore model was used to formulate a hypothesis for inhibitor binding to the RNAP β'-subunit. Attempts to identify a common binding mode for this subset of compounds through standard automated docking on the surface of the β' CH region did not provide any useful result. Multiple solutions were identified for each ligand, with different orientations and amino acid counterparts for hydrophobic and polar interactions. This is likely due to several reasons such as the flat surface of the β' CH region that lacks any recognizable cavity or shaped structural motif capable of accommodating the ligands, and the particular crystal structure utilized for docking experiments in which β' was crystallized with σ^{70}. Therefore, based on the features revealed by the pharmacophore model and their spatial arrangement, we sought to identify a binding site on the surface of the β'-subunit that could provide appropriate binding interactions for the different pharmacophore elements, while also allowing a proper arrangement of the portions of each compound not comprised in the pharmacophore model. We identified Asn294 and Glu295 as β' residues geometrically suitable to act as hydrogen bond donor and acceptor sites for the corresponding acceptor and donor groups of the inhibitors. As highlighted by site-specific mutagenesis studies (*15, 17*), these residues play an important role in the β'-σ^{70} interaction. Moreover, at the top of the CH region, not far from residues Asn294 and Glu295, there is a hydrophobic region potentially capable of accommodating the aromatic moieties of the inhibitors. Individual compounds were thus manually docked on the surface of the β'-subunit in the conformation pointed out by the pharmacophore model and the resulting complexes were energy-minimized in order to remove steric clashes and optimize hydrophobic and polar interactions. As shown in Figure 6C for compound **41**, H-bonds are formed between its carbonyl group and the amide group of Asn294 and between the urea nitrogen and the acidic side chain of Glu295. The hydrophobic 6-fluoro-indole portion is accommodated in the hydrophobic cavity near to the helix-turn-helix motif of β'. The β' portion involved in the interaction with the compound overlaps the region occupied by σ^{70} in the *E. coli* RNAP crystal structure, thus interfering with this essential PPI, RNAPh assembly and transcription. Details on the binding mode of the other β'-σ^{70} inhibitors are reported in Supplementary Figure 6B.

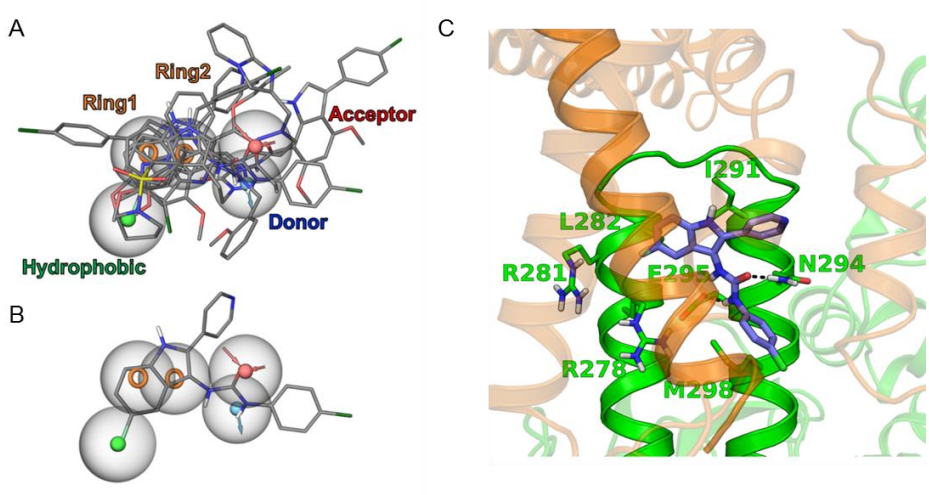

Figure 6. Ligand-based pharmacophore model. (A) Overview of the pharmacophore model. Pharmacophore sites are shown as colored spheres: ring site, orange; hydrophobic site, green; acceptor site, pink; donor site, blue. β'-σ^{70} inhibitors are aligned to the pharmacophore sites. (B) Compound **41** aligned to the pharmacophore model. The indole scaffold matches the two ring sites, the fluorine atom in position 5 occupies the hydrophobic site and the acceptor and donor groups correspond to the urea in the side chain in position 3 of the indole ring. (C) Binding model of compound **41** to the CH region of the RNAP β'-subunit (green ribbons and carbons). The helix corresponding to region 2.2 of the σ^{70} subunit is shown in shaded orange to highlight the portion of the β'-subunit involved in the interaction

There is no obvious relationship between the amino acid sequence of the σ2.2 and β' CH RNAP regions of the four tested bacteria (*E. coli, S. aureus, B. subtilis* and *L. monocytogenes*) and the antibacterial activity of the indol-3-yl-urea derivatives **43** and **47**. In fact, the β' CH and σ2.2 regions are conserved among bacteria, and the species-specific residues of the β' CH region (A286, D289, R293 and L307 in *E. coli* RNAP) are not involved in the β'-σ PPI, nor in the proposed binding mode of the newly discovered PPI inhibitors. Conversely, other amino acid residues within the σ2.2 region (Q400, I410 and M413 in *E. coli* RNAP) are involved in the β'-σPPI and their different chemical identities in the RNAPs from the different tested bacteria might influence the affinity between the two proteins. However, compound internalization, rather than subtle differences in the β'-σ interaction region, is likely to play a more significant (and perhaps dominant) role in affecting the antibacterial activity of the compounds. Regarding the pharmacophore model and the structural hypothesis we propose, it should be noted that, while all the active compounds here identified can interact with Asn294 and Glu295, their precise mode of interaction with RNAP remains to be confirmed by structural data.

CONCLUSION

The virtual screening pipeline coupled with a highly productive yBRET assay, allowed, for the first time, the exploration of an extensive chemical space of candidate interfering compounds and the identification of seven hits, preferentially targeting β'-subunit, out of approximately 5000 candidates selected from a repertoire of ≈34,000 compounds. This experimental set-up, in addition to its sizeable screening throughput (≈800 compounds/day), is also instrumental to: i) pinpointing from the very beginning compounds with at least a minimal capacity to cross biological boundaries (membrane and cell wall) and ii) the early detection of compounds displaying eukaryotic cell toxicity. We believe that the ability to interrogate large compound

libraries and to provide early clues as to the potential biological relevance of the identified compounds are the most attractive features of the yBRET technology. In fact, all of the primary hits identified by yBRET, except the insoluble ones, were confirmed in ELISA, and two out of four displayed at least a minimal growth inhibition capacity. Ultimately, one of these hits led to the identification of two indol-3-yl-urea derivatives (compounds **43** and **47**) that proved highly effective in blocking the growth of Gram-positive bacteria (including the human pathogens *S. aureus* and *L. monocytogenes*) but also *E. coli* upon supplementation of the non-bactericidal membrane permeabilizer PMBN.

A potential improvement of this work would be the targeted modification of some of the present hits in order to improve compounds permeability and to increase their potency. This might be achieved by tailored modulation of chemical structures through synthetic medicinal chemistry, taking advantage of the versatility of the indol-3-yl-urea scaffold. In parallel with chemical modification guided by the β' surface binding hypothesis we have generated, this issue could be addressed by chemical conjugation of β'-σ^{70} PPI inhibitors: i) with antimicrobial peptides or with proteins engaged by bacterial active transport systems (e.g., siderophore transporters) (*36, 37*) to increase the compound permeability, ii) with other RNAP-directed antibiotics targeting distinct regions of the β'-subunit to enhance antibacterial potency while reducing resistance development. Interestingly, a similar dual antibiotic fusion approach has been applied previously to two RNAP-targeting antibiotics (*35*).

Also worth of future investigation will be the identification of novel inhibitors using our ligand-based pharmacophore model as a guideline.

METHODS

Complete descriptions of chemicals, yBRET assay, recombinant protein production, ELISA, molecular modelling, *in vitro* transcription assay, antimicrobial activity assays and statistical analysis are provided in the SI Methods.

SUPPORTING INFORMATION

The Supporting Information is available free of charge on the ACS Publications website at DOI:…
Supplementary figures show: the yBRET and ELISA results for the indole derivatives from the in-house mini library; workflow of the virtual screening procedure, the interaction between the CH region of the β' subunit and region 2.2 of σ^{70}, the pharmacophore model and the minimum energy conformation of reference compound **1;** dose-response curves for the primary hit molecules and the indol-3-yl-urea derivatives; representative gel images documenting the results of *in vitro* transcription inhibition assays; the effect of different concentrations of PMBN on the growth of *E. coli*; ligand-based pharmacophore model and the binding model for hit-compounds interacting with the β' subunit. Reported in supplementary tables are: structures of the indole derivatives from the in-house mini library; the chemical structure and inhibition capacity of indol-3-yl-urea analogs measured by ELISA; compound activity determined by microbial growth inhibition assays; minimum inhibitory concentrations; the results of hemolysis experiments for the two best-performing indol-3-yl-urea analogs; a list of the oligonucleotides employed in this study.

ACKNOWLEDGMENTS

This work was supported by a University of Parma FIL 2014-Young Investigator grant to BM and a grant from the Regione Emilia-Romagna, Italy (Programma di Ricerca Regione-Università 2010–2012; PRUa1RI-2012-006) to SO. We thank the HPC (High Performance Computing) center of the University of Parma for access to the computational facilities and the Interuniversity Consortium for Biotechnologies (CIB) for technical support. The help of M. Simpson (Griffith University) with the handling and delivery of the Compounds Australia selected compound library and technical advice on the *in vitro* transcription assay by C. Rivetti (University of Parma) are also gratefully acknowledged.

DECLARATION OF INTERESTS

We declare that we have no competing interests.

REFERENCES

1. Cima, G. (2014) WHO warns of 'post-antibiotic era', *Journal of the American Veterinary Medical Association 244*, 1356–1357.
2. Allen, H. K., Donato, J., Wang, H. H., Cloud-Hansen, K. A., Davies, J., and Handelsman, J. (2010) Call of the wild: antibiotic resistance genes in natural environments, *Nat Rev Microbiol 8*, 251–259.
3. Brown, E. D., and Wright, G. D. (2016) Antibacterial drug discovery in the resistance era, *Nature 529*, 336–343.
4. Lewis, K. (2016) New approaches to antimicrobial discovery, *Biochem Pharmacol 134*, 87–98.
5. Marston, H. D., Dixon, D. M., Knisely, J. M., Palmore, T. N., and Fauci, A. S. (2016) Antimicrobial Resistance, *Jama 316*, 1193–1204.
6. Ventola, C. L. (2015) The antibiotic resistance crisis: part 1: causes and threats, *P T 40*, 277–283.
7. Boyaci, H., Chen, J., Lilic, M., Palka, M., Mooney, R. A., Landick, R., Darst, S. A., and Campbell, E. A. (2018) Fidaxomicin jams Mycobacterium tuberculosis RNA polymerase motions needed for initiation via RbpA contacts, *eLife 7*.
8. Campbell, E. A., Korzheva, N., Mustaev, A., Murakami, K., Nair, S., Goldfarb, A., and Darst, S. A. (2001) Structural mechanism for rifampicin inhibition of bacterial RNA polymerase, *Cell 104*, 901–912.
9. Lin, W., Das, K., Degen, D., Mazumder, A., Duchi, D., Wang, D., Ebright, Y. W., Ebright, R. Y., Sineva, E., Gigliotti, M., Srivastava, A., Mandal, S., Jiang, Y., Liu, Y., Yin, R., Zhang, Z., Eng, E. T., Thomas, D., Donadio, S., Zhang, H., Zhang, C., Kapanidis, A. N., and Ebright, R. H. (2018) Structural Basis of Transcription Inhibition by Fidaxomicin (Lipiarmycin A3), *Molecular cell 70*, 60–71 e15.
10. Aristoff, P. A., Garcia, G. A., Kirchhoff, P. D., and Showalter, H. D. (2010) Rifamycins--obstacles and opportunities, *Tuberculosis (Edinb) 90*, 94–118.
11. Ho, M. X., Hudson, B. P., Das, K., Arnold, E., and Ebright, R. H. (2009) Structures of RNA polymerase-antibiotic complexes, *Curr Opin Struct Biol 19*, 715–723.
12. Maffioli, S. I., Zhang, Y., Degen, D., Carzaniga, T., Del Gatto, G., Serina, S., Monciardini, P., Mazzetti, C., Guglierame, P., Candiani, G., Chiriac, A. I., Facchetti, G., Kaltofen, P., Sahl, H. G., Deho, G., Donadio, S., and Ebright, R. H. (2017) Antibacterial Nucleoside-Analog Inhibitor of Bacterial RNA Polymerase, *Cell 169*, 1240–1248 e1223.
13. Srivastava, A., Degen, D., Ebright, Y. W., and Ebright, R. H. (2012) Frequency, spectrum, and nonzero fitness costs of resistance to myxopyronin in *Staphylococcus aureus*, *Antimicrob Agents Chemother 56*, 6250–6255.
14. Srivastava, A., Talaue, M., Liu, S., Degen, D., Ebright, R. Y., Sineva, E., Chakraborty, A., Druzhinin, S. Y., Chatterjee, S., Mukhopadhyay, J., Ebright, Y. W., Zozula, A., Shen, J., Sengupta, S., Niedfeldt, R. R., Xin, C., Kaneko, T., Irschik, H., Jansen, R., Donadio, S., Connell, N., and Ebright, R. H. (2011) New target for inhibition of bacterial RNA polymerase: 'switch region', *Curr Opin Microbiol 14*, 532–543.
15. Arthur, T. M., Anthony, L. C., and Burgess, R. R. (2000) Mutational analysis of β' 260–309, a σ^{70} binding site located on *Escherichia coli* core RNA polymerase, *J Biol Chem 275*, 23113–23119.
16. Johnston, E. B., Lewis, P. J., and Griffith, R. (2009) The interaction of *Bacillus subtilis* σ^{A} with RNA polymerase, *Protein Sci 18*, 2287–2297.
17. Ma, C., Yang, X., Kandemir, H., Mielczarek, M., Johnston, E. B., Griffith, R., Kumar, N., and Lewis, P. J. (2013) Inhibitors of bacterial transcription initiation complex formation, *ACS Chem Biol 8*, 1972–1980.
18. Sharp, M. M., Chan, C. L., Lu, C. Z., Marr, M. T., Nechaev, S., Merritt, E. W., Severinov, K., Roberts, J. W., and Gross, C. A. (1999) The interface of σ with core RNA polymerase is extensive, conserved, and functionally specialized, *Genes Dev 13*, 3015–3026.
19. Murakami, K. S. (2013) X-ray crystal structure of *Escherichia coli* RNA polymerase σ^{70} holoenzyme, *J Biol Chem 288*, 9126–9134.
20. Murakami, K. S., Masuda, S., Campbell, E. A., Muzzin, O., and Darst, S. A. (2002) Structural basis of transcription initiation: an RNA polymerase holoenzyme-DNA complex, *Science (New York, N.Y 296*, 1285–1290.

21. Vassylyev, D. G., Sekine, S., Laptenko, O., Lee, J., Vassylyeva, M. N., Borukhov, S., and Yokoyama, S. (2002) Crystal structure of a bacterial RNA polymerase holoenzyme at 2.6 A resolution, *Nature 417*, 712–719.
22. Husecken, K., Negri, M., Fruth, M., Boettcher, S., Hartmann, R. W., and Haupenthal, J. (2013) Peptide-based investigation of the *Escherichia coli* RNA polymerase σ^{70}:core interface as target site, *ACS Chem Biol 8*, 758–766.
23. Ma, C., Yang, X., and Lewis, P. J. (2015) Bacterial Transcription Inhibitor of RNA Polymerase Holoenzyme Formation by Structure-Based Drug Design: From in Silico Screening to Validation, *ACS Infect Dis 2*, 39–46.
24. Corbel, C., Sartini, S., Levati, E., Colas, P., Maillet, L., Couturier, C., Montanini, B., and Bach, S. (2017) Screening for Protein-Protein Interaction Inhibitors Using a Bioluminescence Resonance Energy Transfer (BRET)-Based Assay in Yeast, *SLAS Discov 22*, 751–759.
25. Corbel, C., Wang, Q., Bousserouel, H., Hamdi, A., Zhang, B., Lozach, O., Ferandin, Y., Tan, V. B., Gueritte, F., Colas, P., Couturier, C., and Bach, S. (2011) First BRET-based screening assay performed in budding yeast leads to the discovery of CDK5/p25 interaction inhibitors, *Biotechnol J 6*, 860–870.
26. Corbel, C., Zhang, B., Le Parc, A., Baratte, B., Colas, P., Couturier, C., Kosik, K. S., Landrieu, I., Le Tilly, V., and Bach, S. (2015) Tamoxifen inhibits CDK5 kinase activity by interacting with p35/p25 and modulates the pattern of tau phosphorylation, *Chem Biol 22*, 472–482.
27. Bacart, J., Corbel, C., Jockers, R., Bach, S., and Couturier, C. (2008) The BRET technology and its application to screening assays, *Biotechnol J 3*, 311–324.
28. Chalaye-Mauger, H., Denis, J. N., Averbuch-Pouchot, M. T., and Vallee, Y. (2000) The reactions of nitrones with indoles, *Tetrahedron 56*, 791–804.
29. Di Cesare, M. A., Minetti, P., Tarzia, G., and Spadoni, G. (2003) 5-Halo-tryptamine derivatives used as ligands of the 5-HT6 and/or 5-HT7 serotonin receptors: preparation, and therapeutic use, In *PCT Int. Appl, WO2003000252 A1 20030103*.
30. Mahboobi, S., Teller, S., Pongratz, H., Hufsky, H., Sellmer, A., Botzki, A., Uecker, A., Beckers, T., Baasner, S., Schachtele, C., Uberall, F., Kassack, M. U., Dove, S., and Bohmer, F. D. (2002) Bis(1H-2-indolyl)methanones as a novel class of inhibitors of the platelet-derived growth factor receptor kinase, *J Med Chem 45*, 1002–1018.
31. Mantenuto, S., Lucarini, S., De Santi, M., Piersanti, G., Brandi, G., and Favi, G. (2016) One- pot synthesis of biheterocycles based on indole and azole scaffolds using tryptamines and 1, 2- diaza- 1, 3- dienes as building blocks., *Eur J Org Chem*, 3193–3199.
32. Simpson, M., and Poulsen, S. A. (2014) An overview of Australia's compound management facility: the Queensland Compound Library, *ACS Chem Biol 9*, 28–33.
33. Villoutreix, B. O., Labbe, C. M., Lagorce, D., Laconde, G., and Sperandio, O. (2012) A leap into the chemical space of protein-protein interaction inhibitors, *Curr Pharm Des 18*, 4648–4667.
34. Mielczarek, M., Thomas, R. V., Ma, C., Kandemir, H., Yang, X., Bhadbhade, M., Black, D. S., Griffith, R., Lewis, P. J., and Kumar, N. (2015) Synthesis and biological activity of novel mono-indole and mono-benzofuran inhibitors of bacterial transcription initiation complex formation, *Bioorg Med Chem 23*, 1763–1775.
35. Zhang, Y., Degen, D., Ho, M. X., Sineva, E., Ebright, K. Y., Ebright, Y. W., Mekler, V., Vahedian-Movahed, H., Feng, Y., Yin, R., Tuske, S., Irschik, H., Jansen, R., Maffioli, S., Donadio, S., Arnold, E., and Ebright, R. H. (2014) GE23077 binds to the RNA polymerase 'i' and 'i+1' sites and prevents the binding of initiating nucleotides, *eLife 3*, e02450.
36. Klahn, P., and Bronstrup, M. (2018) Bifunctional antimicrobial conjugates and hybrid antimicrobials, *Natural product reports 34*, 832–885.
37. Schalk, I. J. (2018) Siderophore-antibiotic conjugates: exploiting iron uptake to deliver drugs into bacteria, *Clin Microbiol Infect 24*, 801–802.

FOR TABLE OF CONTENTS ONLY